Proc Indian natn Sci Acad **77** No. 2; (Spl. Issue), June 2011 pp 155-173

Research Paper

Dynamic Response of Piezolaminated Smart Cylindrical Shells with Weak Interfacial Bonding using Three-Dimensional Piezoelasticity

AMIT KUMAR[1], S KAPURIA[2]* and N K GUPTA[2]
[1]*Scientist, Central Mechanical Engineering Research Institute, Durgapur, West Bengal, India*
[2]*Professor, Department of Applied Mechanics, Indian Institute of Technology Delhi, New Delhi 110 016, India*

(Received on 31 January 2011; Revised on 13 April 2011; Accepted on 01 June 2011)

In smart piezoelectric laminated structures, the interfaces between the piezoelectric layers and the host laminate are prone to weak bonding due to the high transverse shear stresses that are induced under electrothermomechanical loading. The weak interfaces may severely affect the actuation and sensing performance and consequently the integrity of the smart structure. In this work, an analytical solution is presented based on the three dimensional piezoelasticity for dynamic response of angle-ply piezolaminated cylindrical shells in cylindrical bending with interlaminar bonding imperfections. The piezoelectric layers are radially polarized and hence useful for structural applications. The discontinuities in displacement, electric and thermal fields at the imperfect interfaces are modelled using a generalized spring layer model. The formulation includes the provision for prescribing potentials at interfaces, which is useful for effective actuation/ sensing. The effect of imperfection on the through-thickness distributions of displacements and stresses, natural frequencies and steady state harmonic response are studied for hybrid composite and sandwich shells. The numerical results will also serve as useful benchmark in assessing simplified theories incorporating interface imperfections.

Key Words: Hybrid Composite; Cylindrical Shell; Weak Interface; Exact Solution; Piezothermoelasticity

1. Introduction

The integration of distributed piezoelectric sensors and actuators in advanced composite structures offers the ability to monitor and/or control the shape, response and health of these structures, which has found application in many engineering systems such as aircrafts, submarines, automobiles and sport products. These laminated structures, however, often suffer from imperfections in bonding between layers that are developed during the manufacturing process and/or service, causing delamination/debonding in the extreme case. The reduction in bonding strength may be due to the degradation or debonding of thin adhesive layer between the adjacent plies. The situation aggravates in the piezoelectric laminates due to high interfacial stresses at the elastic-piezoelectric interfaces. Whereas in elastic laminates the weak bonding affects the structural integrity and response, it significantly alters the required actuation voltages and measured sensory signals in smart piezolaminated (hybrid) structures. This effect, therefore, must be understood and estimated accurately for reliable design of laminated structures as well as of the active control and health monitoring systems. This paper deals with the dynamic response of hybrid piezoelectric angle-ply cylindrical shells with weak interfaces in electrothermomechanical environment.

In case of a non-rigid interface, displacements are not continuous across the interface, while the tractions must be continuous from equilibrium

*Author for Correspondence: kapuria@am.iitd.ac.in; Phone : +91-11-2659-1218 (O); +91-11-2658-1563; Fax: +91-11-2658-1119.

considerations [1]. The transverse displacement discontinuity is likely to cause discontinuity also in the thermal and potential fields across the weak interfaces. The simplest way of modelling the weak interface is to consider that the jumps in the displacements are proportional to the respective tractions, giving rise to the linear shear slip [2-4] and spring layer models [1, 5, 6], which have been frequently employed to model weak bonding in elastic laminates. The effect of bonding imperfections on the response of hybrid piezoelectric beams and plates has been studied using two dimensional (2D) laminate theories [4, 7]. However, analytical solutions based on coupled three dimensional (3D) piezoelasticity are important because these do not make any a priori assumptions on the variations of the field variables across the thickness, and thereby, provide important benchmark to assess the accuracy of simplified 2D theories wherein assumptions are made on the through-thickness distributions of the field variables. Chen and his coworkers presented 3D piezoelasticity solutions for static response of simply supported piezoelectric laminated rectangular plates [8] and cylindrical shells [9] under electromechanical loading, incorporating bonding imperfections using the spring layer model. Their solutions, however, consider that the electric potential can be prescribed only at the surfaces and not at the layer interfaces. The latter case is extremely important in practice though. For example, the interface between the piezoelectric layer and the elastic substrate should be grounded for achieving effective actuation and sensing. Governing differential equations of piezoelasticity for cylindrical shells involve variable coefficients as a function of the radial coordinate. The solution presented in [9] approximates these coefficients to be constant within sublayers. Also, for the cylindrical shell, they considered poling of the piezoelectric layers along the axial direction, whereas effective sensing and actuation in shell structures call for polarization in the radial direction (i.e., the thickness direction). Dumir *et al.* [11] and Kapuria *et al.* [12] presented analytical 3D piezothermoelasticity solutions respectively, for static and dynamic response of perfectly bonded hybrid angle-ply cylindrical shell panels with radially polarized piezoelectric layers, without making the approximation of the coefficients of the differential equations being constant in sublayers. A 3D analytical solution for the static response of hybrid cylindrical shell panels with weak interfaces has been presented [15] using the spring layer model, and the effect of weak bonding on the actuation and sensing authority of piezoelectric layers has been investigated.

This paper presents an analytical solution based on the 3D piezoelasticity for dynamic response of angle-ply hybrid laminated cylindrical shells in cylindrical bending with weak interfacial bonding. The piezoelectric layers are radially polarized. The spring layer model is used for the imperfection, by considering the jump in displacements, electric potential and temperature across the non-rigid interface to be proportional to the associated tractions, transverse electric displacement and heat flux, respectively. The solution includes the case when, besides at inner and outer surfaces, electric potentials are prescribed at layer interfaces also for effective actuation and sensing of piezoelectric layers. The modified Frobenius method [11] is used to solve the system of differential equations with variable coefficients. The effect of imperfect bonding on the static, free vibration and forced vibration response of smart composite shells is illustrated.

2. Governing Equations

Consider an angle-ply laminated circular cylindrical panel (Fig. 1), which is infinitely long and simply-supported at two edges parallel to the axial direction z. The laminate has L layers which can be orthotropic elastic or piezoelectric with orthorhombic class mm2 symmetry with poling along the radial direction. The piezoelectric layers act as distributed actuators and sensors which are surface-bonded or embedded. The span angle, mean radius and total thickness of the shell are denoted by ψ, r_m and h, respectively. The simple supports at $\theta = 0, \psi$ are such that only the radial displacement u is constrained and the tractions along directions θ and z are zero. These ends are electrically grounded and maintained at stress free reference temperature. The thickness and the inner radius of the kth layer numbered from inside are

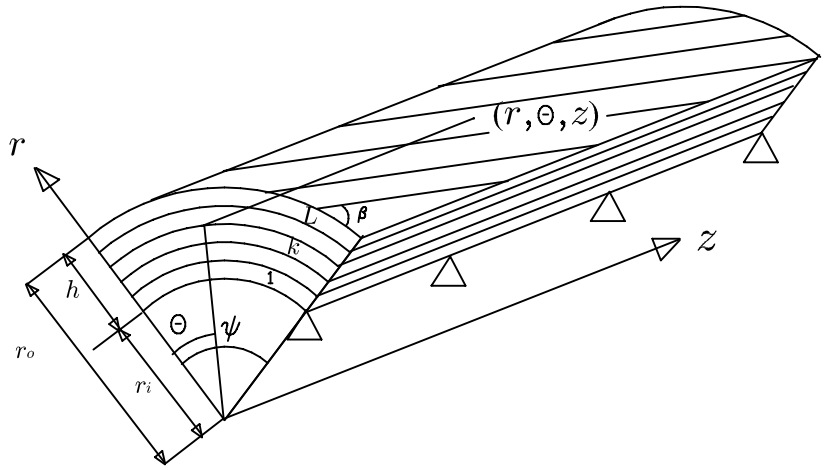

Fig. 1: Geometry and co-ordinates of laminated hybrid cylindrical panel

$t^{(k)}$ and $r_1^{(k)}$. The fibre orientation with respect to θ-axis is $\beta^{(k)}$. The interface between the *k*th and (*k* + 1)th layers is named as the *k*th interface with $r = r_1^{(k+1)}$. Henceforth the layer superscript is omitted unless needed for clarity.

The displacements along r,θ and z directions are denoted by *u*, *v* and *w*, respectively. The panel is subjected to electrothermomechanical load that does not vary along longitudinal coordinate *z*. Thus, all response entities, namely, displacements *v*, *w*, *u*; electric displacements D_θ, D_z, D_r ; electric potential ϕ ; electric field E_θ, E_z, E_r ; temperature rise *T*; strains $\varepsilon_\theta, \varepsilon_z, \varepsilon_r$, $\gamma_{zr}, \gamma_{r\theta}, \gamma_{\theta z}$; and stresses $\sigma_\theta, \sigma_z, \sigma_r$, $\tau_{zr}, \tau_{r\theta}, \tau_{\theta z}$, are independent of *z*. The strain-displacement relations and the electric field-potential relations for this generalized plane strain condition are given by,

$$\begin{aligned} &\varepsilon_\theta = (u + v,\theta)/r, && \gamma_{zr} = w_r, && E_\theta = -\phi_{,\theta}/r \\ &\varepsilon_z = 0, && \gamma_{r\theta} = (u_{,\theta} - v)/r + v_{,r}, && E_z = 0 \\ &\varepsilon_r = u_{,r}, && \gamma_{\theta z} = w_{,\theta}/r, && E_r = -\phi_{,r}, \end{aligned} \quad \ldots (1)$$

A subscript comma denotes differentiation with respect to a spatial coordinate. For the cylindrical coordinate system (r,θ,z) with the material axes x_1 and x_2 at an angle β to the inplane axes θ and *z*, and x_3 along transverse direction *r*, the 3D constitutive equations of a piezoelectric material with class mm2 symmetry are given by:

$$\begin{bmatrix} \varepsilon_\theta \\ \varepsilon_z \\ \varepsilon_r \\ \gamma_{zr} \\ \gamma_{r\theta} \\ \gamma_{\theta z} \end{bmatrix} = \begin{bmatrix} \bar{s}_{11} & \bar{s}_{12} & \bar{s}_{13} & 0 & 0 & \bar{s}_{16} \\ \bar{s}_{12} & \bar{s}_{22} & \bar{s}_{23} & 0 & 0 & \bar{s}_{26} \\ \bar{s}_{13} & \bar{s}_{23} & \bar{s}_{33} & 0 & 0 & \bar{s}_{36} \\ 0 & 0 & 0 & \bar{s}_{44} & \bar{s}_{45} & 0 \\ 0 & 0 & 0 & \bar{s}_{45} & \bar{s}_{55} & 0 \\ \bar{s}_{16} & \bar{s}_{26} & \bar{s}_{36} & 0 & 0 & \bar{s}_{66} \end{bmatrix} \begin{bmatrix} \sigma_\theta \\ \sigma_z \\ \sigma_r \\ \sigma_{zr} \\ \sigma_{r\theta} \\ \sigma_{\theta z} \end{bmatrix} + \begin{bmatrix} 0 & 0 & \bar{d}_{31} \\ 0 & 0 & \bar{d}_{32} \\ 0 & 0 & \bar{d}_{33} \\ \bar{d}_{14} & \bar{d}_{24} & 0 \\ \bar{d}_{15} & \bar{d}_{25} & 0 \\ 0 & 0 & \bar{d}_{36} \end{bmatrix} \begin{bmatrix} E_\theta \\ E_z \\ E_r \end{bmatrix} + \begin{bmatrix} \bar{\alpha}_1 \\ \bar{\alpha}_2 \\ \bar{\alpha}_3 \\ 0 \\ 0 \\ \bar{\alpha}_6 \end{bmatrix} T, \quad \ldots (2)$$

$$\begin{bmatrix} D_\theta \\ D_z \\ D_r \end{bmatrix} = \begin{bmatrix} 0 & 0 & 0 & \bar{d}_{14} & \bar{d}_{15} & 0 \\ 0 & 0 & 0 & \bar{d}_{24} & \bar{d}_{25} & 0 \\ \bar{d}_{31} & \bar{d}_{32} & \bar{d}_{33} & 0 & 0 & \bar{d}_{36} \end{bmatrix} \begin{bmatrix} \sigma_\theta \\ \sigma_z \\ \sigma_r \\ \tau_{zr} \\ \tau_{r\theta} \\ \tau_{\theta z} \end{bmatrix}$$

$$+\begin{bmatrix} \bar{\varepsilon}_{11} & \bar{\varepsilon}_{12} & 0 \\ \bar{\varepsilon}_{12} & \bar{\varepsilon}_{22} & 0 \\ 0 & 0 & \bar{\varepsilon}_{33} \end{bmatrix} \begin{bmatrix} E_\theta \\ E_z \\ E_r \end{bmatrix} + \begin{bmatrix} 0 \\ 0 \\ \bar{q}_3 \end{bmatrix} T, \qquad \text{... (3)}$$

where $\bar{s}_{ij}, \bar{d}_{ij}, \bar{\varepsilon}_{ij}, \bar{\alpha}_i$ and $\bar{q}_3$ are the elastic compliances, piezoelectric strain coefficients, dielectric constants, coefficients of thermal expansion and pyroelectric constant, transformed into the structural coordinate system θ, z, r. The equations of momentum, charge and thermal equilibrium without body force, charge source and heat source are

$$\tau_{r\theta,r} + \sigma_{\theta,\theta}/r + 2\tau_{r\theta}/r = \rho\ddot{v} \qquad \text{... (4)}$$

$$\tau_{zr,r} + \sigma_{\theta z,\theta}/r + 2\tau z_{zr}/r = \rho\ddot{w} \qquad \text{... (5)}$$

$$\sigma_{r,r} + \tau_{r\theta,\theta}/r + (\sigma_r - \sigma_\theta)/r = \rho\ddot{u} \qquad \text{... (6)}$$

$$D_{r,r} + D_r/r + D_{\theta,\theta}/r = 0 \qquad \text{... (7)}$$

$$K_r(T_{,rr} + T_{,r}/r) + k_\theta T_{,\theta\theta}/r^2 = 0 \qquad \text{... (8)}$$

where k_i's $(i = \theta, r)$ are the coefficients of thermal conductivity and an overdot $(\cdot)$ denotes differentiation with respect to time.

3. Boundary Conditions

Dimensionless circumferential coordinate ξ and thickness coordinate $\xi^{(k)}$ for the kth layer are introduced as

$$\xi = \theta/\psi, \zeta^{(k)} = (r - r_1^{(k)})/t^{(k)} \text{ with}$$

$$r_1^{(k)} = r_m - h/2 + \sum_{i=1}^{k-1} t^{(i)} \qquad \text{... (9)}$$

such that ξ and $\xi^{(k)}$ vary from 0 to 1. Let the prescribed harmonic pressure, ambient temperature and the electric potential or the electric displacement at the inner (i =1) and outer (i = 2) surfaces of the shell be $p_i(\xi,t)$, $T_i(\xi,t)$, $\phi_i(\xi,t)$ or $D_i(\xi,t)$, respectively. The panel is subjected to a viscous resistance at the outer surface, proportional to the radial velocity with viscous damping coefficient c_d. Such a damping can model the viscous resistance force of the surrounding medium of the panel. Thus the boundary conditions are:

$$\text{at } \xi = 0,1: \quad u = 0, \ \sigma_\theta = 0,$$

$$\tau_{\theta z} = 0, \quad \phi = 0, \quad T = 0 \qquad \text{... (10)}$$

$$\text{at } r = r_i: \ \sigma_r = -p_1 - c\dot{u}(\xi, r_o, t),$$

$$\tau_{r\theta} = 0, \ \tau_{rz} = 0, \ \phi = \phi_1 \text{ or } D_r = D_1 \qquad \text{... (11)}$$

$$\text{at } r = r_o: \ \sigma_r = -p_2$$

$$\tau_{r\theta} = 0, \ \tau_{rz} = 0, \ \phi = \phi_2 \text{ or } D_r = D_2 \qquad \text{... (12)}$$

$$\text{at } r = r_i: -k_r T_{,r} + h_1 T = h_1 T_1(\xi,t),$$

$$\text{at } r = r_o: -k_r T_{,r} + h_2 T = h_2 T_2(\xi,t) \qquad \text{... (13)}$$

where h_1 and h_2 are the surface heat transfer coefficients at the inner and the outer surfaces of the panel. The special case $h_1 = h_2 = \infty$ corresponds to the temperature of the surfaces being prescribed as T_1 and T_2. The case of known prescribed electric potential $\phi = \phi_i$ at a surface corresponds to the closed circuit electric boundary condition and the case of known electric charge density, $D_r = D_i$ corresponds to the open circuit condition.

4. Modelling Weak Interfaces

For the imperfect interfaces, the displacements, the electric potential as well as the temperature field at the interfaces are discontinuous while the tractions at the interfaces, the radial electric displacement D_r and the heat flux along radial direction are always continuous. The continuity conditions can be expressed as

$$[(\tau_{r\theta}, \tau_{rz}, \sigma_r, D_r)|_{\zeta=1}]^{(k)} = [(\tau_{r\theta}, \tau_{zr}, \sigma_r, D_r)|_{\zeta=0}]^{(k+1)}$$

$$[k_r T_{,\zeta}|_{\zeta=1}/t]^{(k)} = [k_r T_{,\zeta}|_{\zeta=0}/t]^{(k+1)}, \quad k = 1,....,L-1; \qquad \text{... (14)}$$

except for D_r for the interfaces at $k = n_q = 1, ..., L_a$, where the electric potential is prescribed. For actuation of embedded or surface bonded piezoelectric layers, electric potential is prescribed at L_a interfaces. Let the prescribed potential at such an interface n_q be $\Phi_q(\xi)\cos\omega t$. For such interfaces, the continuity condition for D_r in Eq. (14) is to be replaced by the condition

$$\left[\phi\,|_{\zeta=1}\right]^{(n_q)} = \Phi_q(\xi), \qquad q = 1,....,L_a \qquad \text{... (15)}$$

The spring layer model adopted by Chang *et al*. [1] for the displacement field jumps at the imperfect interfaces and by Chen *et al*. [9] for electric potential discontinuity is considered herein also for the thermal field discontinuity. According to this model, the jumps in the displacements (u, v and w), ϕ and T at the weak interfaces are proportional to their respective traction components, D_r and radial heat flow rate, the proportionality constants being spring constant type interface parameters. These continuity conditions can be described as

$$\left[(\sigma_r)\,|_{\zeta=1}\right]^{(k)} = \left[\left[(\sigma_r)\,|_{\zeta=0}\right]^{(k+1)}\right] = K_r^{(k)}[u^{(k+1)} - u^{(k)}],$$

$$\left[(\tau_{\theta r})\,|_{\zeta=1}\right]^{(k)} = \left[\left[(\tau_{r\theta})\,|_{\zeta=0}\right]^{(k+1)}\right] = K_\theta^{(k)}[v^{(k+1)} - v^{(k)}],$$

$$\left[(\tau_{zr})\,|_{\zeta=1}\right]^{(k)} = \left[\left[(\tau_{zr})\,|_{\zeta=0}\right]^{(k+1)}\right] = K_z^{(k)}[w^{(k+1)} - w^{(k)}],$$

$$k = 1,....,L\text{-}1 \qquad \text{... (16)}$$

$$\left[(D_r)\,|_{\zeta=1}\right]^{(k)} = \left[\left[(D_r)\,|_{\zeta=0}\right]^{(k+1)}\right] = K_e^{(k)}[\phi^{(k+1)} - \phi^{(k)}],$$

$$\left[k_r T_{,\zeta}\,|_{\zeta=1}/t\right]^{(k)} = \left[k_r T_{,\zeta}\,|_{\zeta=0}/t\right]^{(k+1)}$$

$$= K_t^{(k)}\left[T^{(k+1)} - T^{(k)}\right]$$

where, $K_i^{(k)}\,(i = r,\theta,z), K_e^{(k)}$ and $K_t^{(k)}$ are the non-negative imperfect interface coefficients for the kth interface for mechanical, electrical and thermal fields, respectively. The dimensionless generalized compliance coefficients, $R_p^{(k)}$, are defined as

$$R_i^{(k)} = c_{11}^{(1)}/[K_i^{(k)}h](i = r,\theta,z),$$

$$R_e^{(k)} = \varepsilon_{33}^{(1)}/[K_e^{(k)}h] \text{ and } R_t^{(k)} = k_r^{(1)}/[K_t^{(k)}h] \qquad \text{... (17)}$$

$R_p^{(k)} = 0$ corresponds to perfect bonding and $R_p^{(k)} = \infty$ indicates complete debonding. A non-zero radial compliance coefficient, R_r, characterizes the radial opening delamination, whereas the shear slip delamination is characterized by non-zero tangential compliance coefficients, R_θ and R_z. For radial opening delamination mode, the radial stress at the interface should not be negative to allow no penetration. The electric and thermal imperfections (i.e. non-zero values of R_e and R_t) are applicable only when radial opening delamination is present.

5. General Solution of Governing Equations

The solution of the governing field equations for the kth layer, satisfying the simply supported boundary conditions (10), is taken in the following Fourier series form:

$$(u,\sigma_r,\sigma_\theta,\sigma_z,\tau_{\theta z},\phi,D_r,T)$$

$$= \sum_{n=1}^{\infty} \Re\,[(u,\sigma_r,\sigma_\theta,\sigma_z,\tau_{\theta z},\phi,D_r,T)_n e^{i\omega t}]\sin n\pi\xi$$

$$(u,w,\tau_{zr},\tau_{r\theta},D_\theta)$$

$$= \sum_{n=1}^{\infty} \Re\,[(v,w,\tau_{zr},\tau_{r\theta},D_\theta)_n e^{i\omega t}]\cos n\pi\xi \qquad \text{... (18)}$$

where, $\Re(\cdots)$ denotes the real part of the complex number $(\cdots)$. For static loading, $\omega = 0$. To satisfy the termwise conditions (11)-(16), the loading functions are similarly expanded as

$$(p_i,\phi_i,D_i,T_i,\Phi_i)$$

$$= \sum_{n=1}^{\infty} \Re\,[(p_i,\phi_i,D_i,T_i,\Phi_i)_n e^{i\omega t}]\sin n\pi\xi \qquad \text{... (19)}$$

Substituting expansion of T from Eq. (18) into

the heat conduction equation (8) yields

$$T_{n,rr} + T_{n,r}/r - \mu_n^2 T_n / r^2 = 0,$$

$$\mu_n = \overline{n}(k_\theta / k_r)^{1/2}, \overline{n} = n\pi/\psi. \quad \text{... (20)}$$

On substitution of the expansions (18), the governing partial differential equations given by Eqs. (1)-(7) reduce to eight first-order ordinary differential equations (ODEs) in terms of 8 independent variables in X_n:

$$X_n = [v_n \;\; w_n \;\; u_n \;\; \sigma_{r_n} \;\; \tau_{zr_n} \;\; \tau_{r\theta_n} \;\; \phi_n \;\; D_{r_n}]^T \quad \text{... (21)}$$

which appear in the boundary and interface conditions given by Eqs. (10)-(16) and five algebraic equations for the remaining variables $\sigma_{\theta_n}, \sigma_{z_n}, \tau_{\theta z_n}, D_{\theta_n}, D_{z_n}$. The algebraic expressions are

$$\sigma_{\theta_n} = p_{11}(\overline{n}v_n - u_n)/r + \overline{n}p_{12}w_n/r + p_{14}\sigma_{r_n} + p_{18}D_{r_n} + t_1 T_n$$

$$\sigma_{z_n} = p_{21}(\overline{n}v_n - u_n)/r + \overline{n}p_{22}w_n/r + p_{24}\sigma_{r_n} + p_{28}D_{r_n} + t_2 T_n$$

$$\tau_{\theta z_n} = p_{61}(\overline{n}v_n - u_n)/r + \overline{n}p_{62}w_n/r + p_{64}\sigma_{r_n} + p_{68}D_{r_n} + t_6 T_n$$

$$D_{\theta n} = \overline{d}_{14}\tau_{zr_n} + \overline{d}_{15}\tau_{r\theta_n} - \overline{n}\overline{\varepsilon}_{11}\phi_n/r$$

$$D_{zn} = \overline{d}_{24}\tau_{zr_n} + \overline{d}_{25}\tau_{r\theta_n} - \overline{n}\overline{\varepsilon}_{12}\phi_n/r \quad \text{... (22)}$$

where $\overline{n} = n\pi/\psi$ and

$$\overline{d}'_{ij} = \overline{d}_{ij}/\overline{\varepsilon}_{33} \quad \overline{s}'_{ij} = \overline{s}_{ij} - \overline{d}_{3i}\overline{d}'_{3j}, \;\; \overline{\alpha}_i = \alpha_i - \overline{d}_{3i}\overline{q}_3/\overline{\varepsilon}_{33}$$

$$p_{i1} = -\hat{s}_{i1}, \;\; p_{i4} = (-\hat{s}_{i1}\overline{s}'_{13} + \hat{s}_{i2}\overline{s}'_{23} + \hat{s}_{i6}\overline{s}'_{36})$$

$$p_{i2} = -\hat{s}_{i6}, \; p_{i8} = (-\hat{s}_{i1}\overline{d}'_{31} + \hat{s}_{i2}\overline{d}'_{32} + \hat{s}_{i6}\overline{d}'_{36})$$

$$t_i = -(\hat{s}_{i1}\overline{\alpha}'_i + \hat{s}_{i2}\overline{\alpha}'_2 + \hat{s}_{i6}\overline{\alpha}'_6) \quad \text{... (23)}$$

$$\begin{bmatrix} \hat{s}_{11} & \hat{s}_{12} & \hat{s}_{16} \\ \hat{s}_{21} & \hat{s}_{22} & \hat{s}_{26} \\ \hat{s}_{61} & \hat{s}_{62} & \hat{s}_{66} \end{bmatrix} = \begin{bmatrix} \hat{s}'_{11} & \hat{s}'_{12} & \hat{s}'_{16} \\ \hat{s}'_{12} & \hat{s}'_{22} & \hat{s}'_{26} \\ \hat{s}'_{16} & \hat{s}'_{26} & \hat{s}'_{66} \end{bmatrix}^{-1}$$

The eight first-order ODEs with variable coefficients can be expressed in matrix form as:

$$X_{n,r} = (A_0 + A_1/r + A_2/r^2)X_n + (Q_0 + Q_1/r)/T_n \quad \text{... (24)}$$

where, matrices A_0, A_1, A_2, Q_0, Q_1 are given by

$$A_0 = \begin{bmatrix} 0 & 0 & 0 & 0 & \overline{s}_{45} & \overline{s}_{55} & 0 & 0 \\ 0 & 0 & 0 & 0 & \overline{s}_{44} & \overline{s}_{45} & 0 & 0 \\ 0 & 0 & 0 & p_4^s + \overline{s}'_{33} & 0 & 0 & 0 & p_8^s + \overline{d}'_{33} \\ -\rho\omega^2 & 0 & 0 & 0 & 0 & 0 & 0 & 0 \\ 0 & -\rho\omega^2 & 0 & 0 & 0 & 0 & 0 & 0 \\ 0 & 0 & -\rho\omega^2 & 0 & 0 & 0 & 0 & 0 \\ 0 & 0 & 0 & p_4^d + \overline{d}'_{33} & 0 & 0 & 0 & p_8^d - 1/\overline{\varepsilon}_{33} \\ 0 & 0 & 0 & & 0 & 0 & 0 & 0 \end{bmatrix}, \quad Q_0 = \begin{bmatrix} 0 \\ 0 \\ \overline{t}_3 \\ 0 \\ 0 \\ 0 \\ 0 \\ 0 \end{bmatrix}$$

$$A_1 = \begin{bmatrix} 0 & 0 & -\bar{n} & 0 & 0 & 0 & -\bar{n}\bar{d}_{15} & 0 \\ 0 & 0 & 0 & 0 & 0 & 0 & -\bar{n}\bar{d}_{14} & 0 \\ \bar{n}p_1^s & \bar{n}p_2^s & -p_1^s & 0 & 0 & 0 & 0 & 0 \\ 0 & 0 & 0 & p_{14}-1 & 0 & \bar{n} & 0 & p_{18} \\ 0 & 0 & 0 & -\bar{n}p_{64} & -1 & 0 & 0 & -\bar{n}p_{68} \\ 0 & 0 & 0 & -\bar{n}p_{14} & 0 & -2 & 0 & -\bar{n}p_{18} \\ \bar{n}p_1^d & \bar{n}p_2^d & -p_1^d & 0 & 0 & 0 & 0 & 0 \\ 0 & 0 & 0 & 0 & \bar{n}\bar{d}_{14} & \bar{n}\bar{d}_{15} & 0 & -1 \end{bmatrix}, \quad Q_1 = \begin{bmatrix} 0 \\ 0 \\ 0 \\ t_1 \\ -\bar{n}t_6 \\ -\bar{n}t_1 \\ t_7 \\ 0 \end{bmatrix} \qquad \text{... (25)}$$

$$A_2 = \begin{bmatrix} 1 & 0 & -\bar{n} & 0 & 0 & 0 & -\bar{n}\bar{d}_{15} & 0 \\ 0 & 0 & 0 & 0 & 0 & 0 & -\bar{n}\bar{d}_{14} & 0 \\ \bar{n}p_1^s & \bar{n}p_2^s & -p_1^s & 0 & 0 & 0 & 0 & 0 \\ 0 & 0 & 0 & p_{14}-1 & 0 & \bar{n} & 0 & p_{18} \\ 0 & 0 & 0 & -\bar{n}p_{64} & -1 & 0 & 0 & -\bar{n}p_{68} \\ 0 & 0 & 0 & -\bar{n}p_{14} & 0 & -2 & 0 & -\bar{n}p_{18} \\ \bar{n}p_1^d & \bar{n}p_2^d & -p_1^d & 0 & 0 & 0 & 0 & 0 \\ 0 & 0 & 0 & 0 & \bar{n}\bar{d}_{14} & \bar{n}\bar{d}_{15} & 0 & -1 \end{bmatrix},$$

with

$$p_i^s = \bar{s}'_{13}p_{1i} + \bar{s}'_{23}p_{2i} + \bar{s}'_{36}p_{6i}$$

$$\bar{t}_3 = \bar{s}'_{13}t_1 + \bar{s}'_{23}t_2 + \bar{s}'_{36}t_6 + \bar{\alpha}'_3$$

$$p_i^d = \bar{d}'_{31}p_{1i} + \bar{d}'_{32}p_{2i} + \bar{d}'_{36}p_{6i}$$

$$\bar{t}_7 = \bar{d}'_{31}t_1 + \bar{d}'_{32}t_2 + \bar{d}'_{36}t_6 + \bar{q}_3/\bar{\varepsilon}_{33} \qquad \text{... (26)}$$

5.1 Solution for the Thermal Problem

Equation (20) represents an Euler-Cauchy type differential equation, whose solution can be obtained in closed form in powers of *r*. But, to obtain the particular solution of Eq. (24) in simple form, the modified Frobenius method [11] is used wherein the solution is expanded in terms of the product of an exponential function and a power series in the dimensionless thickness coordinate ζ: (0 ≤ ≤ 1)

$$T_n(\zeta) = e^{\rho\zeta}\sum_{i=0}^{\infty} T_{n_i}\zeta^i \qquad \text{... (27)}$$

T_n from Eq. (27) is substituted in Eq. (20) and the coefficient of each power of ζ is equated to zero. In the coefficient of ζ^0, setting $T_{n_1} = T_{n_2} = 0$ gives the quadratic characteristic equation for ρ with real roots ρ_1, ρ_2:

$$s\rho^2 + \rho - \mu_n^2/s = 0, \quad s = r_1/t,$$

$$\rho_1, \rho_2 = \left[-1 \pm \left\{1 + 4\mu_n^2\right\}^{1/2}\right]/2s \qquad \text{... (28)}$$

Equating the coefficient of ζ^i to zero for $i > 0$, following recursive relation is obtained for $T_{n_i}^j$ (j = 1, 2).

$$T^j_{n_{i+1}} = -[i(2\rho_j s + 2i - 1)T^j_{n_i} + \{s\rho_j^2\rho_j(4i-3) + \{(i-1)^2 - \mu_n^2\}/s\}T^j_{n_{i-1}} + \{2\rho_j^2 + \rho_j(2i-3)/s\}T^j_{n_{i-2}} + (\rho_j^2/s)T^j_{n_{i-3}}]/si(i+1)], \quad i \geq 2 \quad \text{... (29)}$$

with $T^j_{n-1} = T^j_{n_1} = T^j_{n_2} = 0$. The general solution in terms of arbitrary constants A^n_j is

$$T_n(\zeta) = \sum_{j=1}^{2} e^{\rho_j \zeta}\left(\sum_{i=0}^{\infty} T^j_{n_i}\zeta^i\right)A^n_j \quad \text{... (30)}$$

5.2 Solution for the Coupled Electrothermo-mechanical Problem

The complementary and particular solutions X^c_n and X^p_n of the system of ODEs with variable coefficients given by Eq. (24) are constructed in the same functional form using the modified Frobenius method. Thus, the complementary solution is

$$X^c_n(\zeta) = e^{\lambda\zeta}\sum_{i=0}^{\infty} Z_i\zeta^i \quad \text{... (31)}$$

$$\Rightarrow \quad X^c_{n,r} = e^{\lambda\zeta}\sum_{i=0}^{\infty}[\lambda Z_i + (i+1)Z_{i+1}]\zeta^i/t \quad \text{... (32)}$$

This method differs from the conventional Frobenius method [10] in which the solution is assumed as a product of r^λ and a power series in *r*. It can be readily seen that in the modified method, one term solution in the power series ensures the exact solution of Eq. (24) for the case of constant coefficients with values corresponding to $\zeta = 0$ (i.e. $r = R_1^{(k)}$). Consequently, this method yields much faster convergence compared to the conventional Frobenius and power series methods.

We substitute Eq. (31) these into the homogeneous part of Eq. (24) and equate the coefficient of each power of ζ to zero. Choosing $Z_1 = 0$ in the coefficient of ζ^0 and equating the coefficient to zero yields:

$$AZ_o = \lambda Z_o \quad \text{with} \quad [A_0 r_1 + A_1 + A_2/r_1]/s \quad \text{... (33)}$$

Equation (33) represents an eigenvalue problem of 8 x 8 real matrix *A*, whose solution yields eight pairs of eigenvalue λ_j and eigenvector Z^j_0. Equating the coefficient of ζ^i to zero for $i > 0$ yields the following recursive relation for Z^j_i corresponding to each eigen-pair (λ_i, Z^j_0), $j = 1, ..., 8$:

$$Z^j_{i+1} = [d_0(\lambda_j, i)Z^j_i + d_1(\lambda_j, i)Z^j_{i-1} + d_2(\lambda_j)Z^j_{i-2}]/(i+1), \quad i \geq 1 \quad \text{... (34)}$$

with $d_0(\lambda, i) = A - (\lambda + 2i)/s)I$, $d_1(\lambda, i) = [2r_1A_0 + A_1 - (2\lambda s + i - 1)I]/s^s$, $d_2(\lambda) = (t^{(k)}A_0 - \lambda I)/s^2$ and $Z^j_1 = 0$, $Z^j_{-1} = 0$. The eigenvalues of *A* are either real or occur in complex conjugate pairs. The solution for the complex conjugate pair, however, can be expressed in terms of two real constants [11]. Thus the complete complementary solution $X^c_n(\zeta)$ can be expressed in terms of eight real constants C^n_j as

$$X^c_n(\zeta) = \sum_{j=1}^{8} F^n_j(\zeta)C^n_j \quad \text{... (35)}$$

where, the functional form of $F^n_j(\zeta)$ will depend on the nature of λ_j. The particular solution $X^p_n(\zeta)$ can be constructed in the same form as:

$$X^p_n(\zeta) = \sum_{j=1}^{2} e^{\rho_j\zeta}\left(\sum_{i=0}^{\infty} Y^j_i\zeta^i\right)A^n_j = \sum_{j=1}^{2} G^n_j(\zeta)A^n_j \quad \text{with} \quad G^n_j = e^{\rho_j\zeta}\left(\sum_{i=0}^{\infty} Y^j_i\zeta^i\right) \quad \text{... (36)}$$

where, Y^j_i is obtained from the recursive relation:

$$Y_{i+1}^{j} = [R_1 Q_o + Q_1) s^{-1} T_{n_i}^{j}$$

$$+(2R_1 Q_o + Q_1) s^{-2} T_{n_{i-1}}^{j} + tQ_0 s^{-2} T_{n_{i-2}}^{j}$$

$$+d_0(\rho_j, i) Y_i^j + d_1(\rho_j, i) Y_{i-1}^j + d_2(\rho_j) Y_{i-2}^j]/(i+1) \quad \text{... (37)}$$

with $Y_0^j = 0$ and $Y_{-1}^j = Y_{-2}^j = T_{n_{-1}}^j = T_{n_{-2}}^j = 0$. Thus the general solution of the Eq. (24) is

$$X_n(\zeta) = X_n^c(\zeta) + X_n^p(\zeta)$$

$$= \sum_{j=1}^{8} F_j^n(\zeta) C_j^n + \sum_{p=1}^{2} G_p^n(\zeta) A_p^n \quad \text{... (38)}$$

The infinite power series in $F_j^n(\zeta)$ and $G_p^n(\zeta)$ are truncated to finite number of terms such that the contribution of the first neglected term is less than a stipulated small number η (= 10^{-10}). The $2L$ constants $(A_j^n)^{(k)}$'s for L layers are determined from the $2L$ thermal boundary and interface conditions (13), $(14)_2$ and $(16)_5$. The $8L$ constants $(C_j^n)^{(k)}$ are obtained from the $8L$ boundary and interface conditions (11), (12), (14), (15) and (16). T_n and X_n are then completely determined from Eq. (30) and Eq. (38). Substitution of these entities in Eq. (22) yields D_{θ_n}, D_{z_n}, $\tau_{\theta z_n}$, σ_{θ_n}, σ_{z_n}. The values of various entities are computed at any point using expressions (18) by taking finite number of terms in the fourier series.

For free vibration problem, the system of $8L$ linear algebraic equations for coefficients $(C_j^n)^{(k)}$ is homogeneous. For its nontrivial solution the determinant of the coefficient matrix K of the system of equations is equalled to zero. The roots ω_n of the resulting equation give the undamped natural frequencies. These roots can be obtained numerically using the method of bisection. But, sometimes, it leads to roots which do not satisfy the conditions of zero transverse stresses at inner and outer surfaces. This problem was successfully overcome by using the golden section search method to determine ω for which | det(K) | becomes zero.

6. Numerical Results and Discussions

6.1 Validation

The present formulation and the computer program developed are validated by comparing the results for natural frequencies of an elastic cylindrical panel with imperfect interfaces with the 3D elasticity solution presented by Cai *et al.* [6]. A five layered cylindrical panel of layup [15°/–60°/90°/–75°/45°] (stacking sequence mentioned from bottom to top), with equal thickness for all plies is considered for the purpose. The material properties are considered as : $Y_L/Y_T = 25$, $G_{LT}/Y_T = 0.5$, $G_{TT}/Y_T = 0.2$, $\mu_{LT} = \mu_{TT} = 0.25$. where, Y_i and G_{ij} denote Young's modulus and shear modulus, and ν_{ij} denotes the Poisson's ratio that corresponds to a contraction in direction j when an extension is applied in direction i. Subscripts L

Table 1: Natural frequencies (ω^*) of five layered [15°/–60°/90°/–75°/45°] composite cylindrical panel in cylindrical bending

n	S	$\bar{R} = 0$		$\bar{R} = 0.2$		$\bar{R} = 0.4$	
		Present	Cai *et al.* [6]	Present	Cai *et al.* [6]	Present	Cai *et al.* [6]
1	4	0.8009137	0.800913	0.7451011	0.745101	0.7015897	0.701589
	8	0.6039626	0.603963	0.5785204	0.578520	0.5564013	0.556401
	10	0.5229336	0.522934	0.5061991	0.506199	0.4911400	0.491140
	20	0.2972891	0.297289	0.2941579	0.294158	0.2911329	0.291133
2	8	1.9200775	1.920080	1.7876751	1.787670	1.6841265	1.684130

and T indicate, respectively, directions parallel and perpendicular to the fibres. The span angle of the panel is taken to be $\psi = \pi/3$. The panel has isotropic tangential interfacial imperfection i.e. $\bar{R}^{(k)} = Y_T / hK_\theta^{(k)} = Y_T / hK_Z^{(k)}$, equal at all the interfaces. The dimensionless frequencies $\left(\omega^* = \omega r_i \sqrt{\rho / Y_T}\right)$ for two lower modes n = 1 and 2 for different values of the thickness parameter $S = R/h$ are compared in Table 1. It is observed that the present results match exactly with those of [6].

6.2 Static Response

Results for the static response under electrothermomechanical loading are presented for two simply supported hybrid cylindrical panels (a) and (b) (Fig. 2), each with span angle ψ = 60°. The elastic substrate of panel (a) is a four-layer cross-ply [0°/90°/90°/0°] graphite-epoxy (Gr/Ep) composite while the substrate of panel (b) is made of five-layer [0°/90°/0°/90°/0°] sandwich laminate with composite faces and a soft core. A PZT-5A layer of thickness 0.1h with poling in radial direction is bonded to the outer surface of each panel. The interface between the substrate and the piezoelectric layer is grounded. The material properties are selected as [12].

$[(Y_1, Y_2, Y_3, G_{12}, G_{23}, G_{13}), (\alpha_1, \alpha_2, \alpha_3), (k_1, k_2, k_3), \nu_1, \nu_2, \nu_3]$ = (Gr/Ep): [(181, 10.3, 10.3, 7.17, 2.87, 7.17) GPa, (0.02,22.5,22.5) x $10^{-6}K^{-1}$, (1.5,0.5,0.5) W/mK, 0.28,0.28,0.33]

Face: [(131.1,6.9,6.9,3.588,2.3322,3.588) GPa, (0.0225,22.5,22.5) x $10^{-6}K^{-1}$, (1.5,0.5,0.5)W/mK, 0.32,0.32,0.49]

Core: [(0.2208,0.2001,2760,16.56,455.4,545.1) MPa, (30.6,30.6,30.6) x $10^{-6}K^{-1}$, (3.0,3.0,3.0)W/mK, 0.99, 3 x 10^{-5}, 3 x 10^{-5}]

PZT-5A: [(61.0,61.0,53.2,22.6,21.1,21.1) GPa, (1.5,1.5,2) x $10^{-6}K^{-1}$, (1.8,1.8,1.8)W/mK, 0.35,0.38,0.38] and [(d_{31}, d_{32}, d_{33}, d_{15}, d_{24}), ($\eta_{11}, \eta_{22}, \eta_{33}$)] = [(–171,–171,374,584,584) x 10^{-12} m/V, (1.53,1.53,1,5) x 10^{-8} F/m]

where, η_{ij} denotes the electric permittivities. The following load cases are considered

1. Pressure $p_2 = -p_0 \sin(\pi\theta/\psi)$, applied on the outer surface,

2. Actuation potential $\phi = \phi_0 \sin(\pi\theta/\psi)$ applied at the outer surface,

3. Temperature, $T(h/2) = -T(-h/2) = T_0$, $\sin(\pi\theta/\psi)$.

Outer surfaces of panels are in OC condition $\left(D_r|_{r=r_o} = 0\right)$ for load cases 1 and 3 and in CC condition for load case 2. The results for the above load cases are non-dimensionalised as

Load case 1 : $(\bar{u}, \bar{v}) = 10(u, v) Y_0 / hS^4 p_0$,

$(\bar{\sigma}_\theta, \bar{\tau}_{r\theta}) = (\sigma_\theta, S\tau_{r\theta}) / S^2 p_0$

Load case 2 : $(\bar{u}, \bar{v}) = 10(u, v) S^2 d_0 \phi_0$,

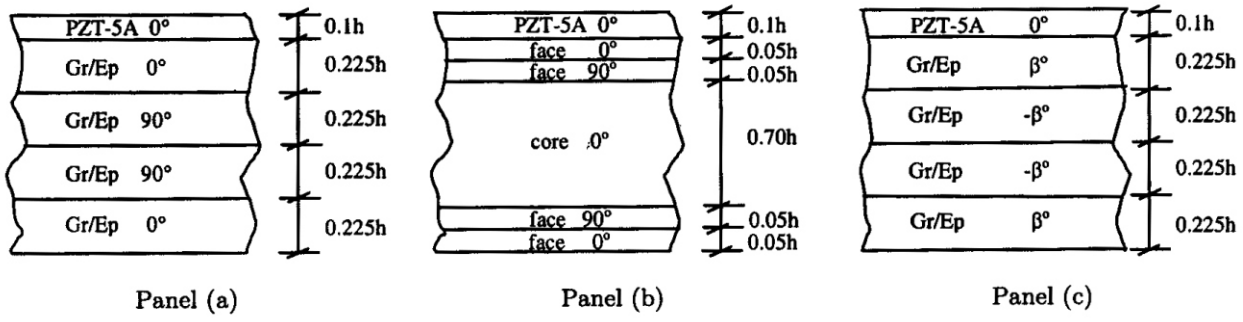

Fig. 2: Layups of hybrid cylindrical panels (a), (b) and (c)

$$(\bar{\sigma}_\theta, \bar{\tau}_{r\theta}) = (\sigma_\theta, S\tau_{r\theta})h/10Y_0 d_0 \phi_0$$

Load case 3 : $(\bar{u}, \bar{v}) = 10(u, v)h\alpha_0 S^2 T_0$,

$$(\bar{\sigma}_\theta, \bar{\tau}_{r\theta}) = 10(\sigma_\theta, S\tau_{r\theta})/\alpha_0 Y_0 T_0$$

where, $S = r_m/h$, $d_0 = 374 \times 10^{-12}$, CN^{-1}. Y_0 and α_0 take values of Y_2 and α_0 of Gr/Ep for panel (a) and of the face for panel (b). The compliance coefficients at an imperfect interface are taken as $R_\theta = R_z = R$. In order to avoid possible material penetration phenomenon at the imperfect interface, R_r and hence R_e and R_t are taken as zero i.e. only shear slip imperfection is considered.

The through-thickness distributions of various entities for the hybrid cross-ply composite and sandwich panels are shown in Figs. 3, 4 and 5 for the pressure, potential and thermal loads (load cases 1, 2 and 3), respectively. For pressure and thermal loads, all the interfaces are considered to have shear slip imperfection with the same value of R. For potential load, only the elastic-piezoelectric interface is considered weak with shear slip imperfection. It may be noted that the discontinuity in the in-plane displacement at the interfaces characterizes slip imperfection behaviour. Plots for the pressure load case show that the presence of imperfection causes an increase in the in-plane displacement $\bar{v}$, deflection $\bar{w}$ and inplane stress $\bar{\sigma}_\theta$ in all layers. But, the transverse shear stress $\bar{\tau}_{r\theta}$ is reduced in middle layers, while increasing in the outer layers. The nature of its variation across the layers changes with the interface compliance. In the hybrid sandwich shell, the imperfection may cause very large increase in $\bar{\tau}_{r\theta}$ in the piezoelectric layers, which is not so in hybrid composite shell. In the case of actuation of the piezoelectric layers (load case 2), the imperfect bonding at piezoelectric-elastic interface prevents the expansion of the piezoelectric layer from being transferred to the elastic substrate through interlaminar shear. As a result, the deflection as well as the inplane normal and shear stresses reduce with imperfection at this interface. Under thermal loading, the presence of imperfect bonding at all interfaces causes an increase in the displacements $\bar{u}$ and $\bar{w}$, and a decrease in the stresses $\bar{\sigma}_\theta$ and $\bar{\tau}_{r\theta}$, as expected. However, no qualitative change due to imperfection is observed in the through-thickness variations of various response entities in the potential and thermal load cases.

6.3 Dynamic Response

For the dynamic response, a hybrid cylindrical panel (c) [Fig. 2] made of a four-layer angle-ply composite substrate and a PZT-5A layer of thickness $0.1h$ bonded to its outer surface is considered. The interface between the substrate and the piezoelectric layer is grounded. To avoid the possible material penetration phenomenon at the imperfect interface, only slip imperfection is considered. The undamped natural frequency ω_n is non-dimensionalized as $\omega_n = \omega_n r_m \; S(\rho_0/Y_0)^{1/2}$ with $Y_0 = 10.3$ GPa and $\rho_0 = 1578$ kg/m^3.

The effect of magnitude and location of imperfection on the undamped natural frequencies is shown in Fig. 6 for the first three modes of vibration of the shell panel with ply angle $\beta = 30^o$, span angle $\psi = 60^o$ and mean radius to thickness ratio $S = 10$. The outer surface of the panel is in closed circuit condition ($\phi|_{r=r_o} = 0$). The plots show that the natural frequencies decrease with the increase in imperfection compliance R, as expected, due to reduction in the bending stiffness of the panel. The change is higher for higher modes. Also, the imperfection at interfaces farther from the surface, has larger effect on the flexural frequencies. Fig. 7 depicts the variation of $\bar{\omega}_n$ with ply angle for the panel with the same imperfection compliance at all interfaces. It is revealed that the reduction in $\bar{\omega}_n$ due to imperfect bonding is higher at lower ply-angles. It is observed from Fig. 8 that the fundamental frequency of shallower shells is more affected by imperfection as compared to deeper shells. The effect of thickness parameter on $\bar{\omega}_n$ of panel (c) with imperfect

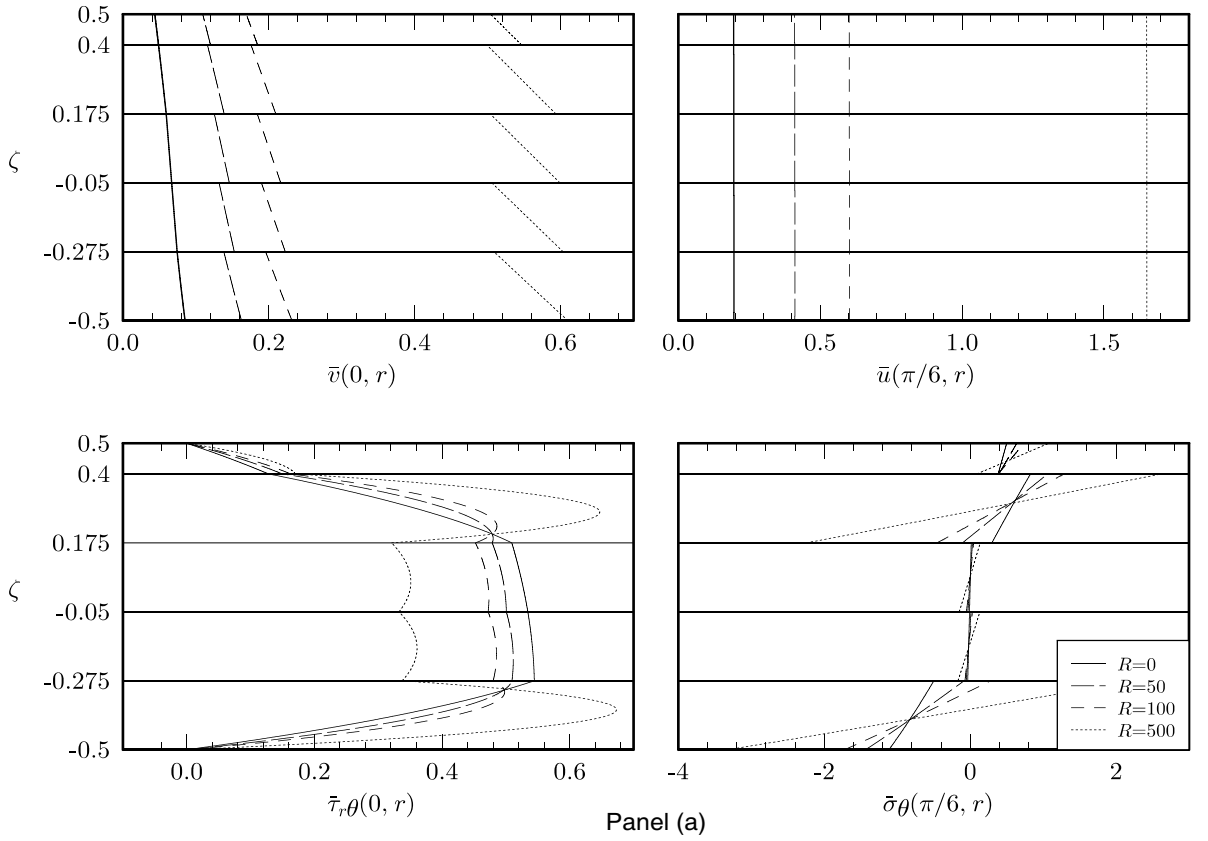

Panel (a)

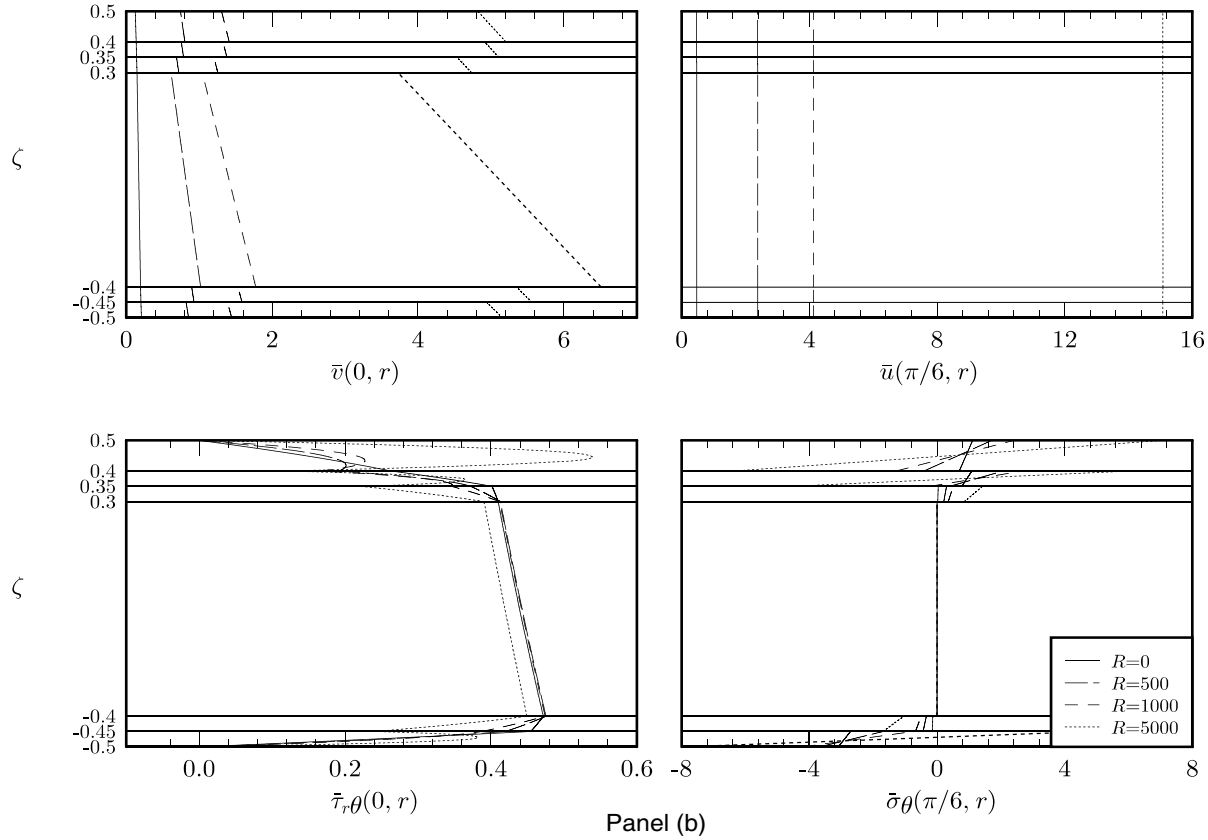

Panel (b)

Fig. 3: Through-the-thickness variations of $\overline{v}, \overline{u}, \overline{\sigma}_\theta$ and $\overline{\tau}_{r\theta}$ for load case 1

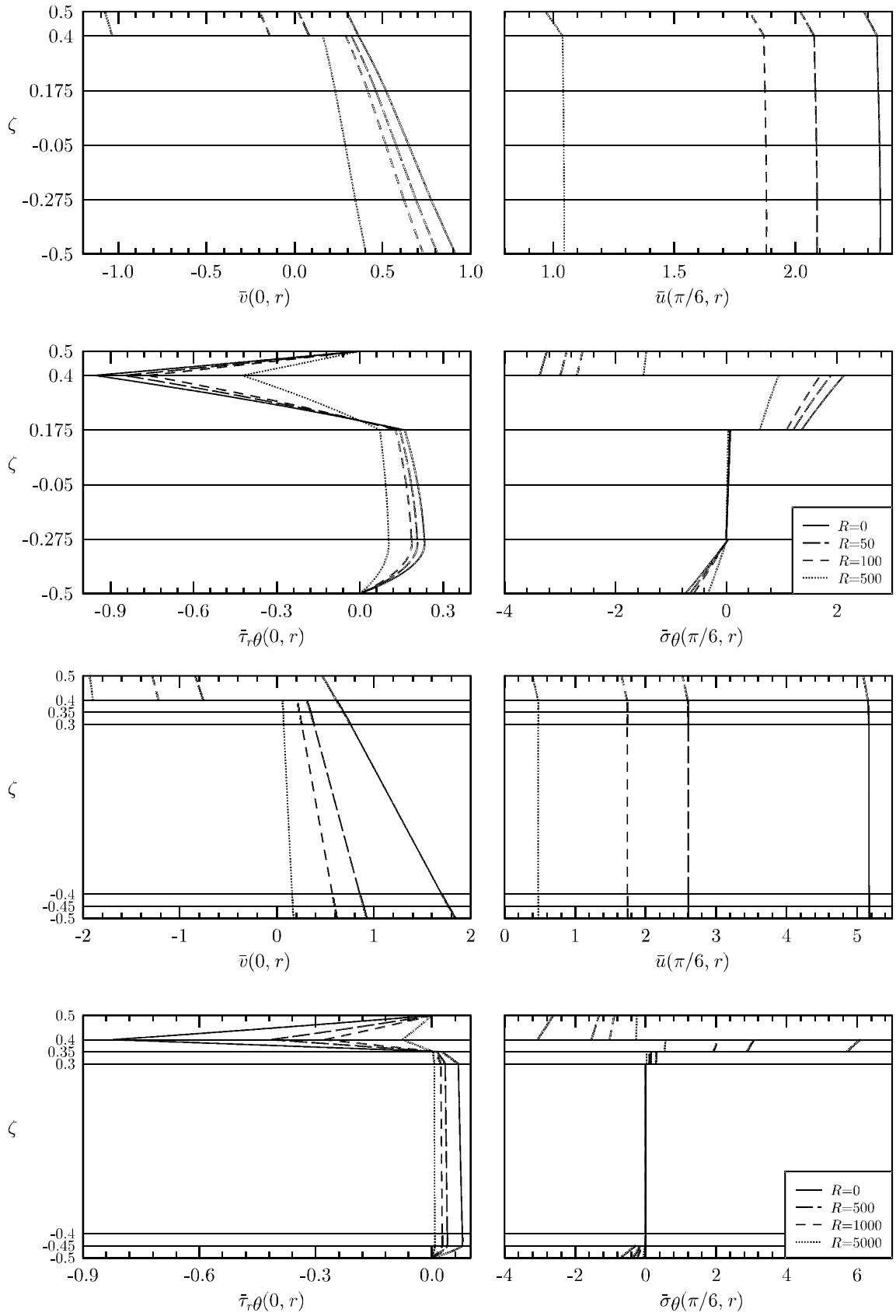

Fig. 4: Through-the-thickness variations of $\overline{v}, \overline{u}, \overline{\sigma}_\theta$ and $\overline{\tau}_{r\theta}$ for load case 2

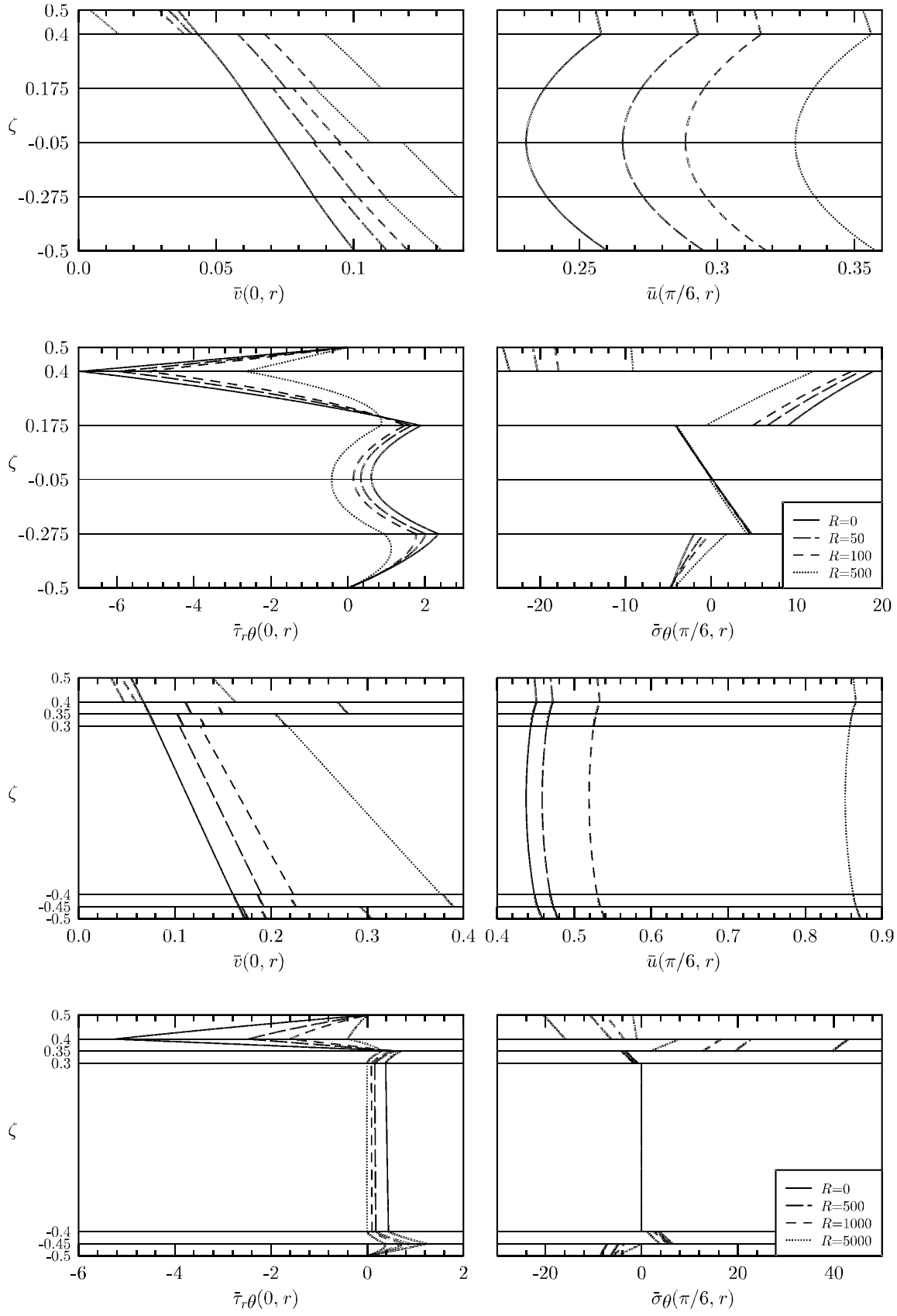

Fig. 5: Through-the-thickness variations of $\overline{v}, \overline{u}, \overline{\sigma}_\theta$ and for load case 3

interfaces is shown in Table 2. For the fundamental frequency, the imperfection has larger effect in thicker shells, but the trend changes in higher modes.

The steady state harmonic response is studied by applying a harmonically varying uniform offset patch load in order to excite multiple modes. Following load cases are considered:

1. Patch pressure $p_2 = -p_0$ applied at outer surface between $\theta = 0.1\psi$ and $\theta = 0.4\psi$.

2. Electric potential $\phi_2 = \phi_0$ applied at outer surface between $\theta = 0.1\psi$ and $\theta = 0.4\psi$.

An uniform imperfection is taken for the pressure load case while only the elastic-piezoelectric interface is considered weak in the potential load case. The results are non-dimensionalized as in Sec. 6.2. The dimensionless damping parameter is defined as $\bar{c} = cS/2\ \rho_0 r_m \omega_1$. The deflection response is

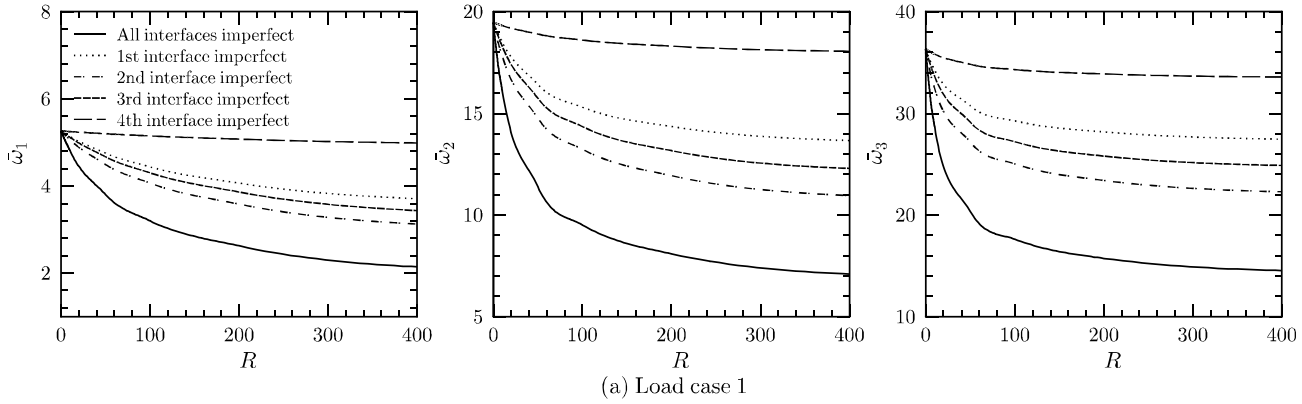

Fig. 6: Effect of magnitude and location of imperfection on natural frequencies $\bar{\omega}_n$ of panel (c)

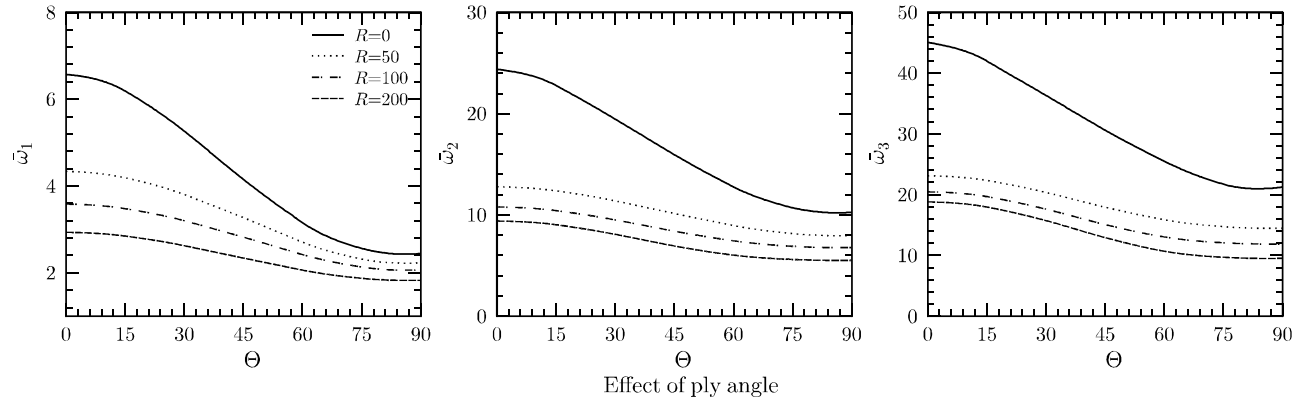

Fig. 7: Effect of ply angle on the imperfection sensitivity of natural frequencies $\bar{\omega}_n$ of panel (c)

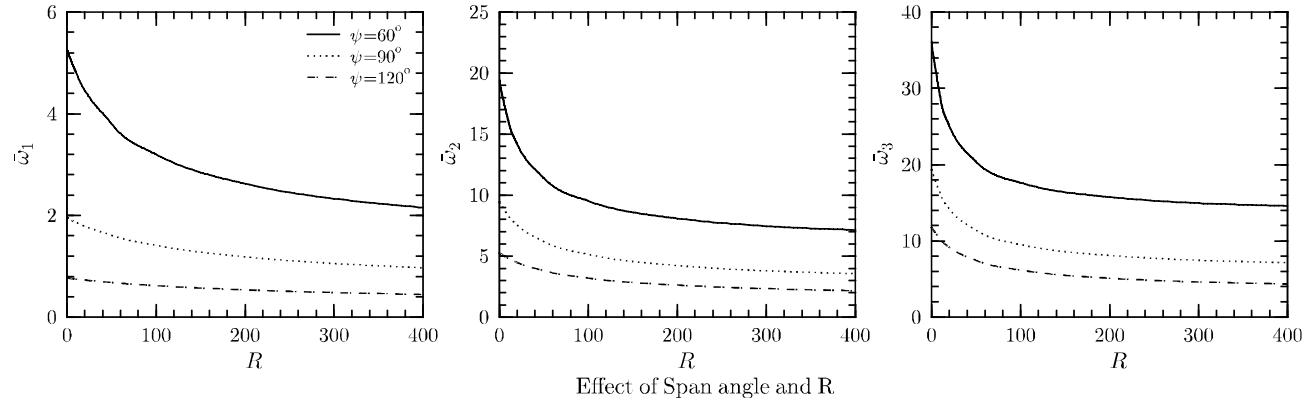

Fig. 8: Effect of span angle on the imperfection sensitivity of natural frequencies $\bar{\omega}_n$ of panel (c)

Table 2: Natural frequencies $\bar{\omega}_n$ of hybrid angle-ply composite panel (c) [$\beta = 30^o, \psi = 60^o$]

n	*S*	*R* = 0	*R* = 50	*R* = 100	*R* = 200
1	5	4.27846	2.50029	2.09013	1.77939
	10	5.26047	3.80321	3.20026	2.62535
	20	5.64834	4.98556	4.52966	3.92999
2	5	13.1066	7.50369	6.72086	6.21860
	10	19.4649	11.3933	9.51598	8.09023
	20	23.9067	17.3148	14.5756	11.9583
3	5	22.2610	13.9274	13.0527	12.5314
	10	36.3036	20.3722	17.6227	15.7376
	20	49.8723	31.5221	26.1133	21.6402

computed at the center of the patch loading ($\theta = 0.25\psi$). Converged results for deflection for the patch loading are obtained with number of Fourier terms N = 30, in both load cases.

The non-dimensionalized steady state amplitude of deflection $\bar{u}_m$ is plotted against the forcing frequency ratio ω/ω_1 in Fig. 9 for undamped ($\bar{c}$ = 0) and damped ($\bar{c}$ = 0.1) vibration of the shell panel under pressure excitation. The panel has ply angle β = 30°, span angle ψ = 60° and S = 10. It is observed that location as well as amplitude (for

Table 3: Deflection amplitude $\bar{u}_m$ of hybrid panel (c) under patch pressure excitation (ω/ω_1 = 0.7)

		$\bar{c} = 0$			$\bar{c} = 0.1$		
R	β	S=5	S=10	S=20	S=5	S=10	S=20
0	30°	0.24496	0.15167	0.12627	0.24387	0.14911	0.11859
	45°	0.36156	0.24107	0.20744	0.35995	0.23702	0.19485
	60°	0.55591	0.41114	0.36966	0.55347	0.40431	0.34739
50	30°	0.71891	0.30189	0.16706	0.71570	0.29689	0.15700
	45°	0.91596	0.40450	0.25089	0.91188	0.39781	0.23576
	60°	1.18160	0.57971	0.41276	1.17640	0.57016	0.38797
100	30°	1.01000	0.42589	0.20533	1.00540	0.41887	0.19304
	45°	1.31690	0.54758	0.29228	1.31100	0.53857	0.27474
	60°	1.70280	0.73640	0.45473	1.69530	0.72434	0.42750
200	30°	1.36810	0.62552	0.27577	1.36190	0.61520	0.25937
	45°	1.88880	0.79434	0.37023	1.88030	0.78130	0.34817
	60°	2.55800	1.02490	0.53599	2.54670	1.00820	0.50407

Table 4: Deflection amplitude of hybrid panel (c) under patch potential excitation (ω/ω_1 = 0.7)

		$\bar{c} = 0$			$\bar{c} = 0.1$		
R	β	S=5	S=10	S=20	S=5	S=10	S=20
0	30°	2.72800	2.34900	2.20630	2.71670	2.31180	2.07870
	45°	3.97050	3.58950	3.43490	3.95390	3.53240	3.23650
	60°	5.57350	5.35750	5.26800	5.55030	5.27280	4.96540
50	30°	1.66290	1.96860	2.09470	1.65570	1.93670	1.97270
	45°	2.64890	3.10790	3.29290	2.63750	3.05760	3.10160
	60°	4.16730	4.85860	5.12390	4.14940	4.78090	4.82850
100	30°	1.21140	1.72080	1.99960	1.20610	1.69270	1.88250
	45°	2.02250	2.77420	3.16850	2.01370	2.72900	2.98360
	60°	3.38960	4.47900	4.99190	3.37490	4.40680	4.70310
200	30°	0.76480	1.39000	1.84340	0.76152	1.36710	1.73470
	45°	1.36350	2.30900	2.95870	1.35760	2.27110	2.78500
	60°	2.47990	3.90940	4.75890	2.46910	3.84590	4.48220

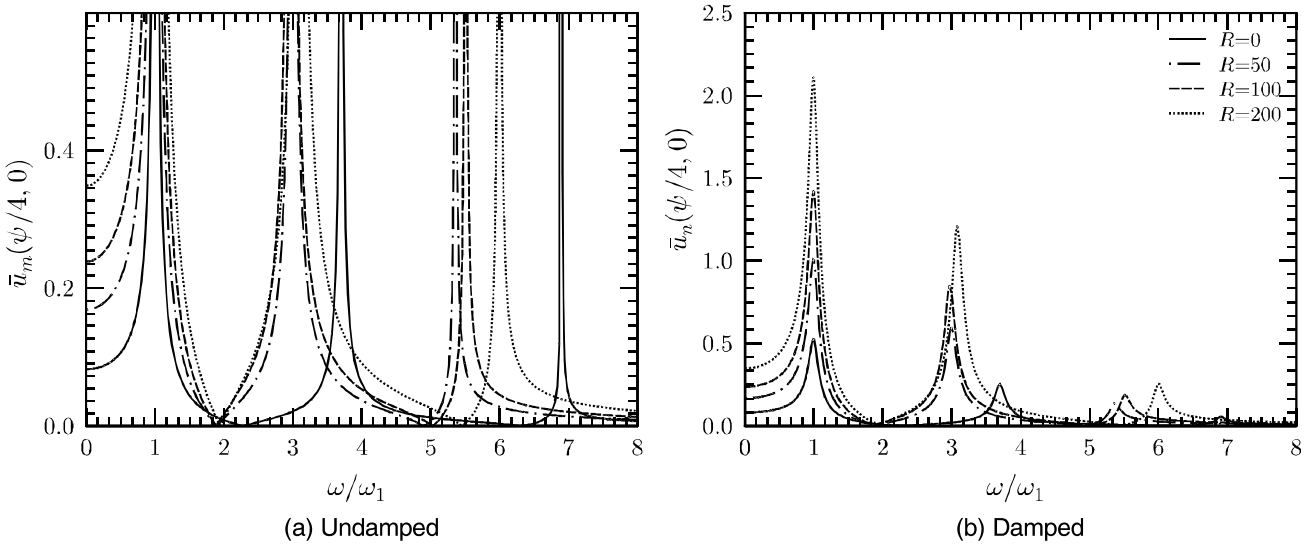

Fig. 9: Deflection amplitude of hybrid shell panel (c) under harmonic patch pressure load

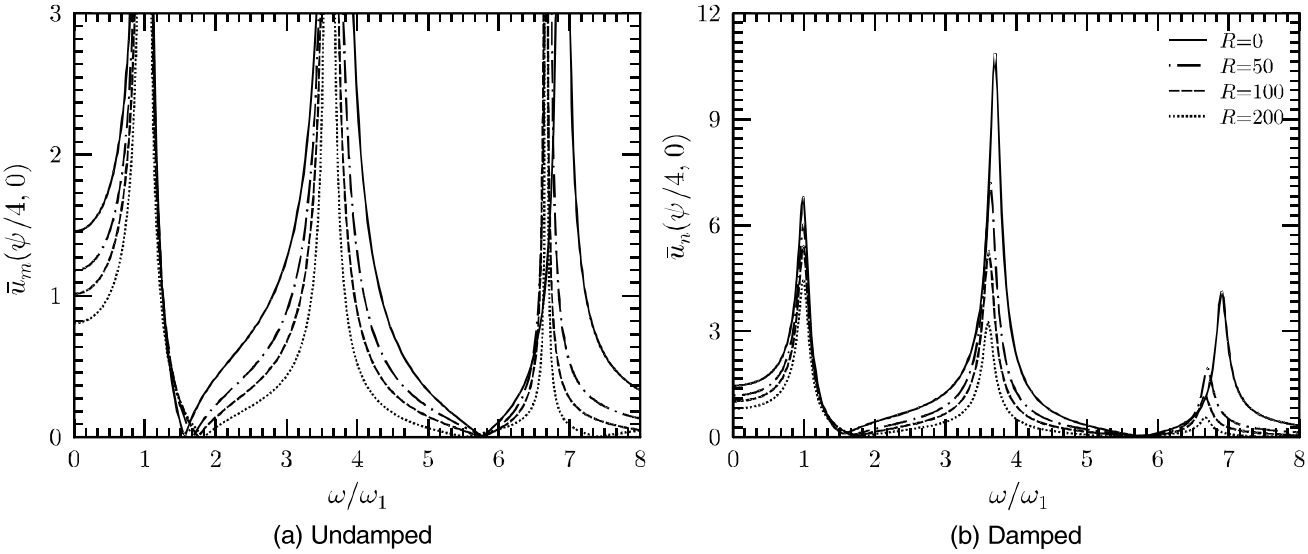

Fig. 10: Deflection amplitude of hybrid shell panel (c) under harmonic patch potential load

damped case) of peaks of the frequency response curves change significantly with increasing imperfection, particularly for higher modes. Similar curves for the potential load case are plotted in Fig. 10. Here, the shift of the peaks in higher modes is not as significant.

The effect of weak bonding on the steady state amplitude of vibration of the shell for harmonic excitation of cases 1 and 2 is illustrated in Fig. 11. Steady state deflection amplitudes $\tilde{u}_m$ of the weakly bonded panel under harmonic excitations with forcing frequency $\omega = 0.8\,\omega_1$, normalized with respect to those without imperfection, is plotted against R for different values of β, ψ and S. Unless otherwise specified, $\beta = 30^o$, $\psi = 60^o$ and $S = 10$. The deflection amplitude increases with imperfection for the pressure load case and decreases for the potential load case, the rate of change being higher for smaller ply angles, smaller span angles and thicker shells, for both the load cases.

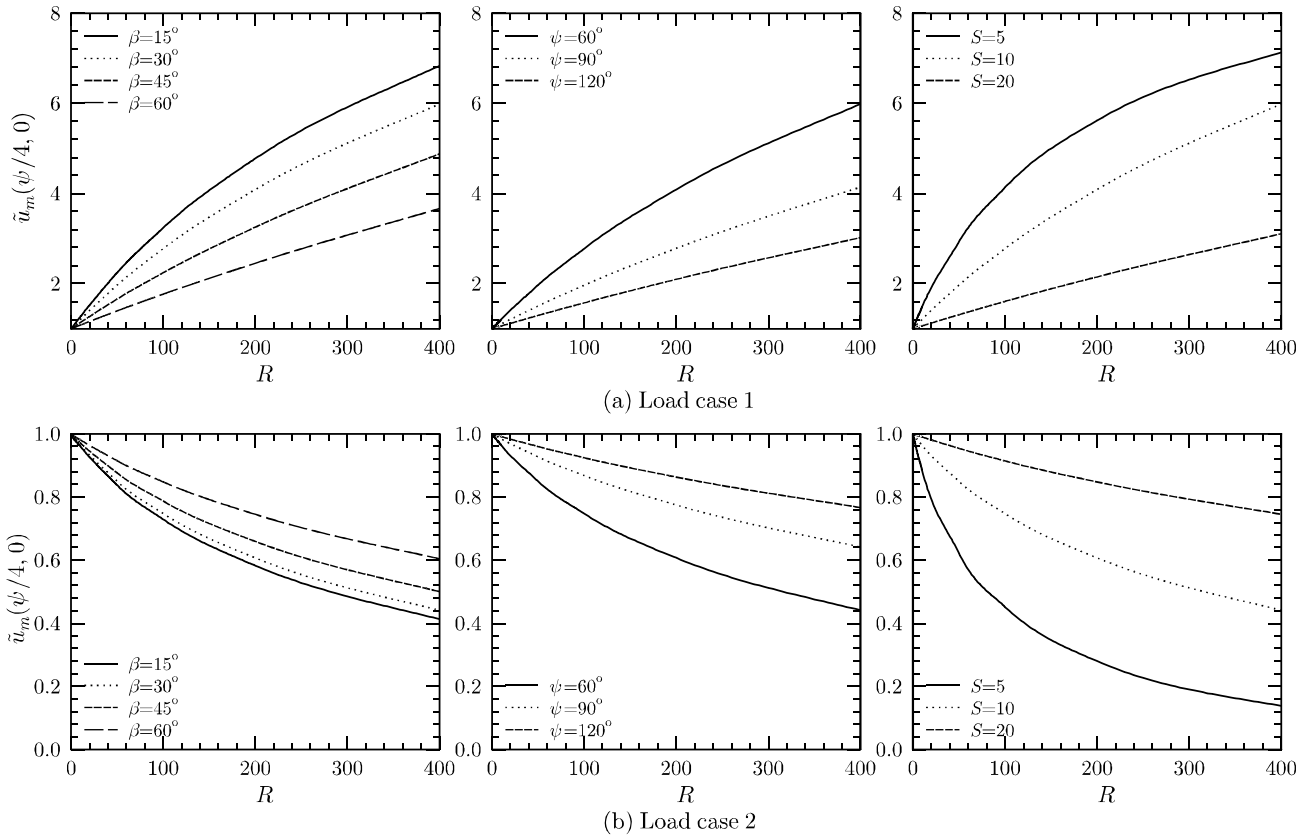

Fig. 11: Effect of weak bonding on steady state deflection amplitude of hybrid shell panel (c) under harmonic pressure and potential loads

The dimensionless amplitudes of deflection $\bar{u}_m$ for the hybrid shell (c) with span angle 60°, with and without damping, are presented in Tables 3 and 4, respectively for load cases 1 and 2 of forcing frequency ratio $\omega/\omega_1 = 0.7$, for different values of R, β and S. These tabulated results can be used as benchmarks in assessing the accuracy of 2D theories and other approximate 3D solutions.

7. Conclusions

A 3D piezothermoelasticity solution is presented for free vibration and forced harmonic response of simply supported hybrid piezoelectric cylindrical panels in cylindrical bending with imperfect interfaces. The weak interlaminar bonding is modelled by the generalized spring layer model. The piezoelectric layers are radially polarized unlike some existing solutions, wherein axial polarization is assumed which is ineffective for structural applications. The results presented herein will provide important benchmark for assessing the accuracy of simplified 2D theories for smart shells with weak interfaces. The numerical results reveal that the change in the fundamental frequency for a given imperfection compliance is higher for lower ply-angles, shallower and thicker shells. Consequently, the rate of change in the steady state deflection amplitude with imperfection compliance is higher for smaller ply angles, smaller span angles and thicker shells, for pressure and potential excitations with forcing frequencies close to the fundamental frequency. But the same trend may not hold well for higher modes. The nature of variation of stresses across the elastic and piezoelectric layers may change due to imperfection, which should be accounted for in the design of such smart structures.

8. Acknowledgements

The second and third authors gratefully acknowledge the support for carrying out this work through DST-RFBR Project Grant No. INT/RFBR/P-24.

References

1. Cheng ZQ, Jemah AK and Williams FW *J Appl Mech* **63** (1996) 1019-26
2. Lu X and Liu D *AIAA J* **30** (1992) 1063-1073
3. Di M Sciuva, Icardi U and Librescu L *Int J Fract* **96** (1999) 17-35
4. Icardi U, Di M Sciuva and Librescu L *AIAA J* **38** (2000) 499-506
5. Chen W Q and Lee K Y *Compos Struct* **64** (2004) 275-283
6. Cai J B, Chen W Q and Ye G R *Comps Sci Tech* **64** (2004) 1753-1762
7. Seeley C E and Chattopadhyay A *Int J Solids Struct* **36** (1999) 1823-1843
8. Chen W Q, Cai J B, Ye G R and Wang Y F *Int J Solids Struct* **41** (2004) 5247-5263
9. Chen W Q and Lee K Y *Arch Appl Mech* **74** (2005) 466-476
10. Kreyszig E *Advanced Engineering Mathematics* Wiley India, New Delhi (1999)
11. Dumir P C, Dube G P and Kumar S *J Intell Mat Sys Struct* **8** (1997) 452-464
12. Kapuria S, Kumari P and Nath J K *J Sound Vib* **324** (2009) 832-849
13. Xu K M, Noor A K *AIAA J* **34** (1996) 802-812
14. Heyliger P *Int J Solids Struct* **34** (1997) 3781-3794
15. Kapuria S and Amit Kumar *Proc of SPIE* **7644** (2010)